Direct probing of acylperoxy radicals during ozonolysis of α-pinene: constraints on radical chemistry and production of highly oxygenated organic molecules

Han Zang[1], Dandan Huang[2], Jiali Zhong[3], Ziyue Li[1], Chenxi Li[1], Huayun Xiao[1], Yue Zhao[1,*]

[1]School of Environmental Science and Engineering, Shanghai Jiao Tong University, Shanghai, 200240, China

[2]Shanghai Academy of Environmental Sciences, Shanghai 200233, China

[3]Division of Environment and Sustainability, Hong Kong University of Science and Technology, Hong Kong SAR, 999077, China

*Correspondence: Yue Zhao (yuezhao20@sjtu.edu.cn)

Abstract

Acylperoxy radicals (RO_2) are key intermediates in atmospheric oxidation of organic compounds and different from the general alkyl RO_2 radicals in reactivity. However, direct probing of the molecular identities and chemistry of acyl RO_2 remains quite limited. Here, we report a combined experimental and kinetic modelling study of the composition and formation mechanisms of acyl RO_2, as well as their contributions to the formation of highly oxygenated organic molecules (HOMs) during ozonolysis of α-pinene. We find that acyl RO_2 radicals account for 67%, 94%, and 32% of the highly oxygenated C_7, C_8, and C_9 RO_2, respectively, but only a few percent of C_{10} RO_2. The formation pathway of acyl RO_2 species depends on their oxygenation level. The highly oxygenated acyl RO_2 (oxygen atom number ≥ 6) are mainly formed by the intramolecular aldehydic H-shift (i.e., autoxidation) of RO_2, while the less oxygenated acyl RO_2 (oxygen atom number < 6) are basically derived from the C-C bond cleavage of alkoxy (RO) radicals containing an α-ketone group or the intramolecular H-shift of RO containing an aldehyde group. The acyl RO_2-involved reactions explain 50-90% of C_7 and C_8 closed-shell HOMs and 14% of C_{10} HOMs, respectively. For C_9 HOMs, this contribution can be up to 30%-60%. In addition, acyl RO_2 contribute to 50%-95% of C_{14}-C_{18} HOM dimer formation. Because of the generally fast reaction kinetics of acyl RO_2, the acyl RO_2 + alkyl RO_2 reactions seem to outcompete the alkyl RO_2 + alkyl RO_2 pathways, thereby affecting the fate of alkyl RO_2 and HOM formation. Our study sheds lights on the detailed formation pathways of the monoterpene-derived acyl RO_2 and their contributions to HOM formation, which will help to understand the oxidation chemistry of monoterpenes and sources of low-volatility organic compounds capable of driving particle formation and growth in the atmosphere.

1. Introduction

Monoterpenes ($C_{10}H_{16}$) comprise an important fraction of nonmethane hydrocarbons in the global atmosphere (Guenther et al., 2012; Sindelarova et al., 2014) and make a significant contribution to the secondary organic aerosol (SOA) budget (Pye et al., 2010; Iyer et al., 2021). The presence of double bond and large molecular size of monoterpenes favor their oxidation reactivity towards O_3, hydroxyl (OH), and nitrate (NO_3) radicals (Atkinson et al., 1990; Roger et al., 2004; Kurten et al., 2015; Kristensen et al., 2016; Bianchi et al., 2019; Berndt, 2022), as well as the formation of low-volatility products and SOA (Fry et al., 2009; Fry et al., 2014; Zhang et al., 2018; Bianchi et al., 2019; Molteni et al., 2019; Shen et al., 2022). The organic peroxy radicals (RO_2) in the gas-phase oxidation of monoterpenes can undergo autoxidation and form a class of highly oxygenated organic compounds (HOM) (Jokinen et al., 2014; Mentel et al., 2015; Berndt et al., 2016; Zhao et al., 2018; Bianchi et al., 2019; Bell et al., 2021; Berndt, 2022), which are primarily low- or extremely low-volatility organic compounds (LVOCs and ELVOCs) (Ehn et al., 2014; Bianchi et al., 2019) and thus play a crucial role in SOA formation and growth.

Significant advances have been made in recent years concerning the monoterpene RO_2 autoxidation and its contribution to HOM formation (Ehn et al., 2014; Berndt et al., 2016; Zhao et al., 2018; Xu et al., 2019; Lin et al., 2021; Berndt, 2022; Shen et al., 2022). It is recognized that a part of monoterpene RO_2 radicals derived from the traditional ozonolysis channel (i.e., isomerization of Criegee intermediates, CI) and OH addition channel can autoxidize at a rate larger than 1 s^{-1} and could be an important contributor to HOM formation (Zhao et al., 2018; Xu et al., 2019; Berndt, 2021). Recently, new reaction channels leading to the RO_2 radicals that can undergo fast autoxidation have been proposed. A quantum chemical calculation study indicated that an excited CI arising from α-pinene ozonolysis could undergo ring-breaking reactions and directly lead to a ring-opened RO_2 due to the excess energy, which can autoxidize at a rate of ~1 s^{-1} and rapidly form highly oxidized RO_2 with up to 8 oxygen atoms (Iyer et al., 2021). In addition, the minor hydrogen abstraction channel by OH radicals has been proposed as a predominant pathway to HOM formation from OH oxidation of α-pinene under atmospheric conditions (Shen et al., 2022).

RO_2 species can be simply divided into alkyl RO_2 and acyl RO_2 (RC(O)OO) according to whether R is an acyl radical. There are significant differences in the reactivity of these two kinds of RO_2. Firstly, the rate constant of acyl RO_2 with NO is in general slightly higher than that of alkyl RO_2 (Atkinson et al., 2007; Calvert et al., 2008; Orlando and Tyndall, 2012). For example, the reaction rate constants of acyl RO_2, $CH_3C(O)O_2$, and alkyl RO_2, $CH_3CH_2O_2$, with NO have been reported to be 20×10^{-12} cm^3 $molecule^{-1}$ s^{-1} and 9.2×10^{-12} cm^3 $molecule^{-1}$ s^{-1}, respectively (Atkinson et al., 2007;

Calvert et al., 2008; Orlando and Tyndall, 2012). Besides, acyl RO_2 can react rapidly with NO_2 and form thermally unstable peroxyacyl nitrates ($RC(O)OONO_2$), which have a lifetime of tens of minutes at room temperature and of days and even months in winter or in the upper atmosphere with lower temperatures (Atkinson et al., 2007; Orlando and Tyndall, 2012). Although alkyl RO_2 radicals can also react with NO_2 and form the alkyl peroxynitrates ($ROONO_2$), they are extremely unstable and will decompose into RO_2 radicals and NO_2 in less than 1s (Kirchner et al., 1997; Orlando and Tyndall, 2012). Lastly, the rate constant of cross-reaction of acyl RO_2 ($1.5 \pm 0.3 \times 10^{-11}$ cm^3 $molecule^{-1}$ s^{-1}) is significantly higher than that of alkyl RO_2 (2×10^{-17} - 1×10^{-11} cm^3 $molecule^{-1}$ s^{-1}) (Villenave and Lesclaux, 1996; Tyndall et al., 2001; Atkinson et al., 2007; Zhao et al., 2018). As a result, these two kinds of RO_2 may play different roles in the autoxidation as well as HOM and dimer formation.

The quantum calculations revealed that different functional groups in RO_2 would lead to significantly different intramolecular H-shift rates (Otkjær et al., 2018). The C=O and C=C substituents lead to resonance stabilized carbon radicals and could enhance the H-shift rate constants by more than a factor of 400. The fast aldehydic H-shift rate contributes to a series of acyl radicals (RC(O)) with the radical site at the terminal carbonyl carbon, which further produce the acyl RO_2 with O_2 addition. Many RO_2 formed in the oxidation of monoterpenes have the aldehyde functionality, especially for α-pinene ozonolysis, in which all the primary and many later-generation RO_2 contain at least one aldehyde group (Noziere et al., 2015; Berndt et al., 2018; Li et al., 2019; Berndt, 2022; Zhao et al., 2022). As a result, acyl RO_2 may comprise a considerable fraction of total RO_2 species and contribute significantly to the formation of low-volatility products and SOA in the monoterpene oxidation system. A recent study by Zhao et al. (2022) found that the acyl RO_2-involved reactions contribute to 50%-80% of oxygenated C_{15}-C_{20} dimers (O:C $\geq$ 0.4) and 70% of C_{15}-C_{19} dimer esters in SOA from α-pinene ozonolysis. However, currently the direct probing of the molecular identities and chemistry of monoterpene-derived acyl RO_2 radicals is rather limited. The role of acyl RO_2 in HOM formation remains to be quantified.

In this study, the molecular identities and formation mechanisms of acyl RO_2 radicals, as well as their contributions to HOM formation in the α-pinene ozonolysis are investigated. The experiments were conducted in a flow reactor with different concentrations of NO_2, which acted as an efficient scavenger for the acyl RO_2. The molecular composition and abundance of the gas-phase HOMs were measured by a chemical ionization-atmospheric pressure interface-time-of-flight mass spectrometer (CI-APi-TOF) using nitrate as the reagent ions. In addition, kinetic modelling using the Framework for 0-D Atmospheric Modeling (F0AM v4.1) employing Master Chemical

Mechanisms (MCM v3.3.1) updated with the latest advances of the RO_2 chemistry was performed to gain insights into the reaction kinetics and mechanisms of acyl RO_2 species. We find that acyl RO_2 account for a major fraction of highly oxygenated C_7 and C_8 RO_2 and play a significant role in the formation of HOM monomers and dimers with small molecular size. This study will help to understand the role of acyl RO_2 in the formation of low-volatility species from monoterpene oxidation and reduce the uncertainties in the future atmospheric modelling of the formation and impacts of aerosols.

2. Method and Materials

2.1 Flow Reactor Experiments.

The α-pinene ozonolysis experiments were carried out under room temperature (298 K) and dry conditions (relative humidity < 5%) in a custom-built flow reactor, which has been described in detail previously (Yao et al., 2019). The α-pinene vapor was generated by evaporating its pure liquid (99%, Sigma-Aldrich) into a flow of zero air (10.65 L min^{-1}) added to the reactor using an automated syringe pump (TYD01-01-CE, Baoding Leifu Fluid Technology Co., Ltd.). The initial concentrations of α-pinene ranged from 500 ppb to 3 ppm in different experiments. Ozone was generated by passing a flow of ultra-high-purity (UHP) O_2 (150 mL min^{-1}, Shanghai Maytor Special Gas Co., Ltd.) through a quartz tube housing a pen-ray mercury lamp (UV-S2, UVP Inc.) and its concentration (45 ppb and 180 ppb under low and high O_3 conditions, respectively) was measured by an ozone analyzer (Model 49i, Thermo Fisher Scientific, USA). The NO_2, acting as an acyl RO_2 scavenger, was derived from its standard cylinder gas (15.6 ppm, Shanghai Weichuang Standard Gas Co., Ltd.) and its initial concentration ranged from 0 to 30 ppb. To validate the formation mechanisms of acyl RO_2, selected experiments with the addition of NO or cyclohexane were also conducted. NO was derived by its standard cylinder gas (9.8 ppm, Shanghai Weichuang Standard Gas Co., Ltd.) and its initial concentration also ranged from 0 to 30 ppb. The gas-phase cyclohexane (~ 500 ppm), acting as an OH scavenger, was generated by bubbling a gentle flow of UHP N_2 through liquid cyclohexane (LC-MS grade, CNW). The total air flow in the flow reactor was 10.8 L min^{-1} and the residence time was 25 seconds. The relatively low O_3 concentration and short reaction time in the flow reactor avoid significant production of NO_3 radicals from NO_2 and O_3 and make the NO_3 oxidation contribute only 0.3%-1.2% of the total α-pinene oxidation in our experiments. Therefore, the NO_3 chemistry could be neglected in this study. A summary of the experimental conditions is given in Tables S1 and S2 in the Supplement.

The gas-phase RO_2 radicals and closed-shell products were measured by a nitrate-based CI-API-TOF mass spectrometer (abbreviated as nitrate-CIMS; Aerodyne Research, Inc.), and a long time-

of-flight mass spectrometer with a mass resolution of ~10000 Th/Th was used here. The mass calibration error is below 1.8 ppm. The sheath flow, including a 2 mL min^{-1} UHP N_2 flow containing nitric acid (HNO_3) and 22.4 L min^{-1} zero air was guided through a PhotoIonizer X-ray (Model L9491, Hamamatsu, Japan) to generate nitrate reagent ions. The total sample flow rate was 9 L min^{-1} during the experiments. The mass spectra within the m/z range of 50 to 700 were analyzed using the tofTools package developed by Junninen et al. (2010) based on Matlab.

To clarify whether there is SOA formation in the experiments, a scanning mobility particle sizer (SMPS, TSI), which consists of an electrostatic classifier (model 3080), a long or nano differential mobility analyzer (model 3081 and 3085 for different particle sizes), and a condensation particle counter (model 3087), was used to monitor the formation of SOA particles. Except in Exp 31 where the reacted α-pinene reached 36.8 ppb and there was low SOA formation with particle mass concentrations of 5.0×10^{-4}-5.7×10^{-3} μg m^{-3} and number concentrations of 63-395 cm^{-3}, no particle formation was observed by SMPS. Therefore, the RO_2 radicals and closed-shell products would be primarily distributed in the gas phase, with their fates negligibly influenced by the low SOA formation under these experimental conditions.

2.2 Kinetic Model Simulations.

Model simulations of RO_2 and HOM formation in selected experiments were performed to constrain the reaction kinetics and mechanisms of acyl RO_2 using F0AM v4.1 (Wolfe et al., 2016), which employs MCM v3.3.1 (Jenkin et al., 2015) updated with the chemistry of RO_2 autoxidation and cross-reactions forming HOM monomers and dimers. Newly added species and reactions to MCM v3.3.1 followed the work by Zhao et al. (2018) and Wang et al. (2021). Considering that the default MCM v3.3.1 does not include highly oxygenated acyl RO_2, we added the possible formation pathways of the potential acyl RO_2 measured in this study to the model based on the mechanisms proposed by Zhao et al. (2022).

The formation and reaction branching ratios of the two α-pinene-derived CIs are updated in the model according to the recent studies (Table S3) (Claflin et al., 2018; Iyer et al., 2021; Zhao et al., 2021; Berndt, 2022). The formation of a ring-opened $C_{10}H_{15}O_4$-RO_2 species (C10H15O4RBRO2 in Table S3) from α-pinene ozonolysis proposed by a recent study (Iyer et al., 2021), as well as its subsequent autoxidation and bimolecular reactions, is included in the model. The autoxidation rate constant of the ring-opened $C_{10}H_{15}O_4$-RO_2 is 1 s^{-1}, and a lower limit of its molar yield (30%) was used according to the recent studies (Zhao et al., 2021; Meder et al., 2023) and our results (see details in Section 3.3). We also added the hydrogen abstraction channel of α-pinene oxidation by OH radicals according to a recent study (Shen et al., 2022). The branching ratio of this channel was

set to 9%, with the rest 91% being the traditional OH addition pathways. The detailed reaction pathways and rate constants of RO_2 species in this channel followed the work by Shen et al. (2022), except for RO_2 cross-reactions, the rates of which were not reported in that study. As the primary RO_2 radicals ($C_{10}H_{15}O_2$-RO_2) formed via the hydrogen abstraction by OH radical are least-oxidized with only 2 oxygen atoms, their cross-reaction rate could be relatively low (Atkinson et al., 2007; Orlando and Tyndall, 2012). In the model, this rate constant was set to 1×10^{-13} cm^3 $molecule^{-1}$ s^{-1}. For other alkyl RO_2 radicals (including HOM-RO_2), their cross-reaction rate constant is assumed to be 1×10^{-12} cm^3 $molecule^{-1}$ s^{-1} according to Zhao et al. (2018). The dimer formation rates for these alkyl RO_2 are same as their cross-reaction rates.

In flow reactor experiments, the equilibrium formation of $ROONO_2$ would lead to the consumption of alkyl RO_2 radicals. To account for the influence of this process on the RO_2 budget and HOM formation, we included the reaction of $RO_2 + NO_2 \leftrightharpoons ROONO_2$ in the model, with forward and reverse reaction rate constants of 7.5×10^{-12} cm^3 $molecule^{-1}$ s^{-1} and 5 s^{-1}, respectively (Orlando and Tyndall, 2012). To simply the parameterization, the forward and reverse reaction rate constants of newly added highly oxygenated acyl RO_2 with NO_2 are the same as default values in MCM v3.3.1. Besides, the cross-reaction rate constants of acyl RO_2 (including acyl RO_2 + acyl RO_2 and acyl RO_2 + alkyl RO_2) forming monomers or dimers were both set to 1×10^{-11} cm^3 $molecule^{-1}$ s^{-1} (Orlando and Tyndall, 2012). Considering that there are large uncertainties in the dimer formation rate of RO_2, a sensitivity analysis was conducted to evaluate its influence on acyl RO_2-involved HOM formation by varying the rate constant from 1×10^{-13} cm^3 $molecule^{-1}$ s^{-1} to 1×10^{-12} cm^3 $molecule^{-1}$ s^{-1} for alkyl RO_2 and 1×10^{-12} cm^3 $molecule^{-1}$ s^{-1} to 1×10^{-11} cm^3 $molecule^{-1}$ s^{-1} for acyl RO_2. The results show that changes in dimer formation rate constants within the above ranges have no significant influence on the contribution of acyl RO_2 to HOM formation (Figure S1).

The wall losses of OH, HO_2, and RO_2 radicals, as well as closed-shell HOM monomers and dimers in the flow reactor were considered using the KPS method proposed by Knopf et al. (2015) in the model (Table S4), with an assumption of irreversible uptake of these species on the reactor wall. It is found that the wall loss of OH, HO_2, and RO_2 radicals accounts for 0.08-0.14%, 4.7-9.1%, and 7.3-25.5% of their total production, respectively, with lower values under higher reacted α-pinene concentration conditions. Therefore, the wall loss process would not significantly influence α-pinene oxidation and RO_2 chemistry. The wall losses of closed-shell HOM monomers and dimers account for 18.4-34.7% and 14.2-33.1% of their total production, respectively. It should be noted that the wall losses of typical RO_2 and HOMs have negligible impact on their responses to the addition of NO_2 (Figure S2). In addition, with the consideration of the wall loss effects, the effect

and contribution of acyl RO_2 to the HOM formation only changed a little (0.02-0.5%). Therefore, the wall losses of RO_2 and HOMs in the flow reactor would not affect the interpretation of the results in this study.

3. Results and Discussion

3.1 Molecular composition of acyl RO_2 from α-pinene ozonolysis

The overall formation characteristics of gas-phase RO_2, closed-shell monomers, and dimers with the addition of NO_2 (30 ppb) is shown in Figure 1 (Exps 8 and 14, Table S1). Since nitrate-CIMS is only highly sensitive to the highly oxygenated species, we only discuss the production of HOMs with oxygen atoms above 6 here. As for RO_2 and closed-shell monomers (Figure 1a), the signals of C_7 and C_8 species decrease by more than 50% with the addition of NO_2, while for C_9 and C_{10} species, their decreases are relatively small (within 40%). In addition, we note that there is an unexpected increase in some C_9 and C_{10} RO_2, and the possible reason will be discussed in detail in Section 3.3.

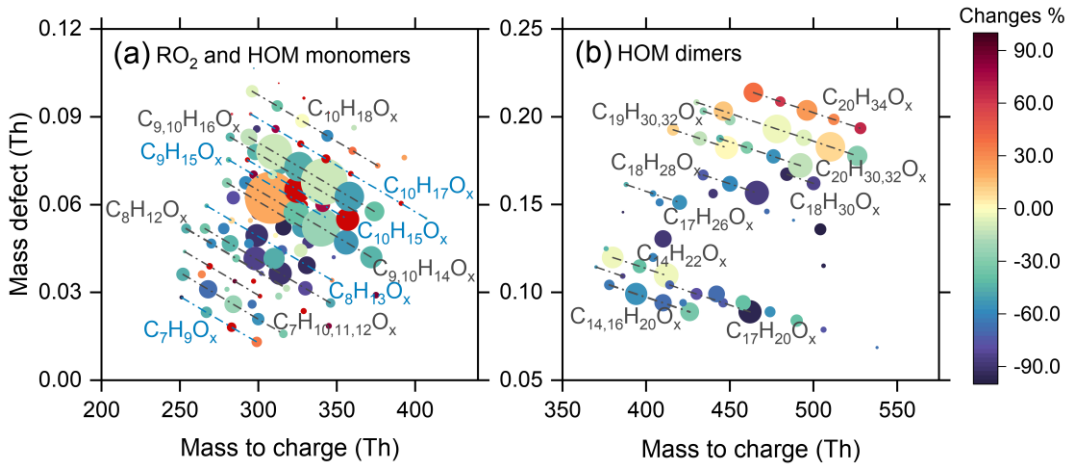

Figure 1 Mass defect plots of (a) RO_2, HOM monomers, and (b) HOM dimers formed from ozonolysis of α-pinene in the presence of NO_2 measured using nitrate-CIMS (Exps 8, 14). The circles are colored by the relative changes in signal of RO_2, monomers and dimers due to the addition of NO_2 (30 ppb). The area of circles is linearly scaled with the cube root of the signal of HOMs formed in the absence of NO_2. The blue lines represent RO_2 radicals.

NO_2 could react rapidly with acyl RO_2 radicals to form $RC(O)OONO_2$, which has a higher thermal-stability compared to $ROONO_2$ and can serve as a sink for acyl RO_2 on our experimental timescales. Therefore, a significant decrease in C_7 and C_8 RO_2 and HOMs upon the addition of NO_2 indicates that a major fraction of C_7 and C_8 RO_2 are acyl RO_2. In contrast, the slight decrease in C_9 and C_{10} HOM monomers shows that the contribution of acyl RO_2 to C_9 and C_{10} RO_2 is relatively small. However, some of the C_{10} monomers showed a slight increase with the addition of NO_2, especially

for $C_{10}H_{18}O_x$-HOMs. The addition of NO_2 plays a twofold role in dimer formation from α-pinene ozonolysis (Figure 1b). There is a significant inhibiting effect on C_{14}-C_{18} dimers, which is due to the large contribution of acyl RO_2 to the total C_7 and C_8 RO_2 that generate such dimers. However, C_{19} and C_{20} dimers only show a slight decrease with the addition of NO_2, and some of them are even enhanced. In particular, the enhancement in $C_{20}H_{34}O_x$ is most significant, reaching 30%.

Kinetic model simulations show that the concentration of alkyl RO_2 decreases by 1-20% with the addition of 30 ppb NO_2 under different reacted α-pinene conditions (Exps 1-28). Considering that the acyl RO_2 could be rapidly consumed by NO_2, if the signal reduction of a RO_2 specie significantly exceeds 20% with 30 ppb NO_2 addition, we presume it has significant contribution from acyl RO_2. As a result, a total of 10 acyl RO_2 were identified according to the changes of RO_2 signal as a function of initial NO_2 concentration, which include $C_7H_9O_6$, $C_7H_9O_7$, $C_8H_{13}O_6$, $C_8H_{13}O_8$, $C_8H_{13}O_9$, $C_8H_{13}O_{10}$, $C_9H_{13}O_9$, $C_9H_{17}O_7$, $C_9H_{17}O_9$, and $C_{10}H_{15}O_7$. Figure 2 shows the averaged normalized acyl RO_2 signals measured as a function of the added NO_2 concentration under different experimental conditions (Exps 1-28). Similarly, since nitrate-CIMS is only highly sensitive to products with high oxygen content, we only observed acyl RO_2 with oxygen atoms above 6. Consistent with the significant decrease in C_7 and C_8 species with the addition of NO_2 in Figure 1a, C_7 and C_8 acyl RO_2 decrease by more than 50% with the increase of NO_2 concentration (Figures 2a, b). For C_9 acyl RO_2, the $C_9H_{17}O_7$-RO_2 and $C_9H_{17}O_9$-RO_2 also decrease dramatically with increasing NO_2, and the decrease in $C_9H_{13}O_9$-RO_2 is relatively smaller (Figure 2c). In addition, $C_{10}H_{15}O_7$-RO_2 also shows a small decrease (Figure 2d), with a reduction of only 30% at 30 ppb NO_2. The relatively small reduction in the abundance of some of these RO_2 radicals indicates the presence of alkyl RO_2 radicals with the same chemical formulas. Along with the marked reduction in acyl RO_2 signals, the production of highly oxygenated $RC(O)OONO_2$ species such as $C_9H_{13}O_9NO_2$, $C_9H_{17}O_7NO_2$, and $C_{10}H_{15}O_7NO_2$ with the addition of NO_2 were observed (see the spectra in Figure S3). However, we note that although some $RC(O)OONO_2$ such as $C_8H_{13}O_6NO_2$ and $C_8H_{13}O_8NO_2$ are expected to be formed with NO_2 addition, they could not be unambiguously detected by nitrate-CIMS due to the overlapping of their peaks with strong alkyl RO_2 peaks ($C_9H_{15}O_8$-RO_2 and $C_9H_{15}O_{10}$-RO_2) in this study.

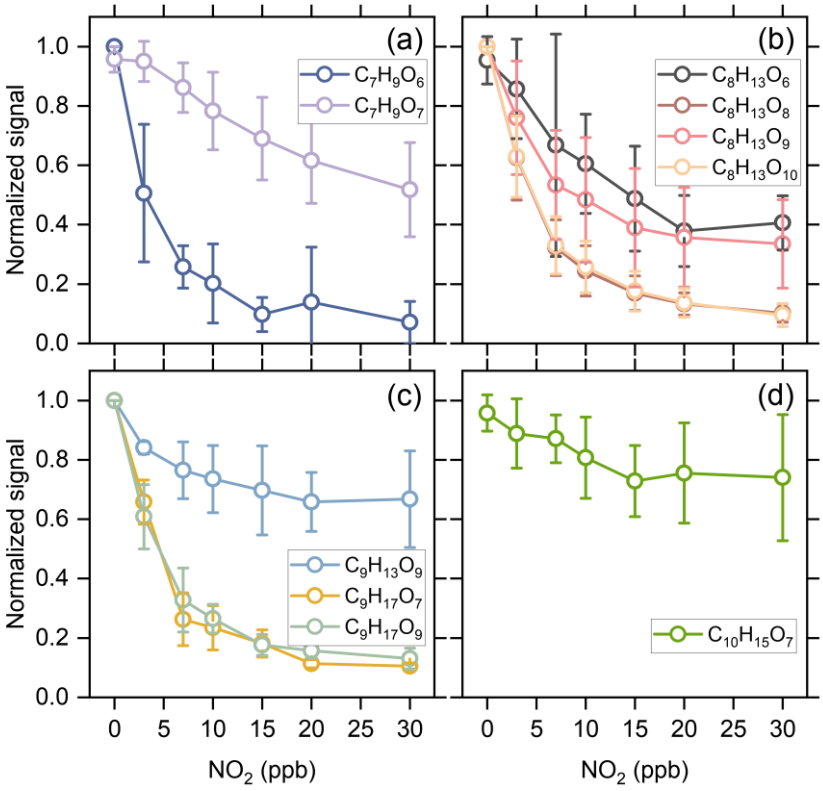

Figure 2 Averaged normalized signal of the measured acyl RO_2 as a function of the added NO_2 concentration under different experimental conditions (Exps 1-28).

Figure 3 shows the contribution of acyl and alkyl RO_2 to the highly oxidized C_7-C_{10} RO_2. Acyl RO_2 contribute 66.9%, 94.3% and 31.7% to the total C_7, C_8, and C_9 RO_2 signals, respectively. By contrast, the only C_{10} acyl RO_2 measured in this study is $C_{10}H_{15}O_7$, which contributes to only 0.4% of the total C_{10} RO_2. It should be note that there might be other C_{10} acyl RO_2 that were not observed due to the interferences from the alkyl RO_2 with the same chemical formulas, which respond differently to the addition of NO_2 than acyl RO_2 do (see details in the following discussion). Considering that some RO_2 formulas such as $C_{10}H_{15}O_7$ may have contributions from both acyl RO_2 and alkyl RO_2, we assumed the decrease of RO_2 signal with the addition of NO_2 as the signal of acyl RO_2. Besides, it is obvious that the normalized signal basically decreases to the lowest value when the initial NO_2 concentration reaches 10 ppb (Figure 2), indicating that most of the acyl RO_2 are depleted at this NO_2 concentration. In addition, the decreasing extents of some acyl RO_2 are different for different reacted α-pinene concentrations, with lower decreasing extent for higher reacted α-pinene concentrations (Figure S4). This difference might be due to the promoted cross-reactions of acyl RO_2 as well as their precursor RO_2 at higher α-pinene concentrations, which are competitive with the reactions leading to acyl RO_2 formation as well as the acyl RO_2 + NO_2 reactions.

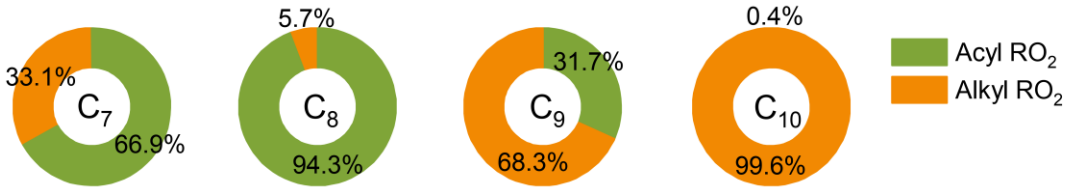

Figure 3 Contributions of acyl and alkyl RO_2 to the highly oxygenated C_7-C_{10} RO_2 measured by nitrate-CIMS.

In addition to the changes of acyl RO_2 signal, we also show the changes of normalized alkyl RO_2 signal with the increasing initial NO_2 concentration in Figure S5. Although $ROONO_2$ formed by the reaction of alkyl RO_2 with NO_2 is thermally unstable and would decompose quickly to release RO_2, it would still reach a formation/decomposition equilibrium in the system, thus consuming a small amount of alkyl RO_2. However, it can be seen from Figure S5 that during 25 s of reaction in the flow reactor, a large part of alkyl RO_2 has an increasing trend with the increase of NO_2 concentration. We speculate that a portion of $ROONO_2$ could decompose back to RO_2 and NO_2 in the nitrate-CI inlet where the sample gases were diluted instantly and the equilibrium of $ROONO_2$ was disturbed, resulting in the release of a large amount of RO_2.

To verify our speculation, the decomposition of $ROONO_2$ in the CI inlet was simulated based on the dilution ratio (1:3.5) and residence time (200 ms) in the inlet. As shown in Figure S6, more than 40% of $ROONO_2$ decompose back to RO_2 and NO_2 in the CI inlet, which would inevitably lead to an increase in RO_2 concentration. As the $C_{10}H_{15}O_8NO_2$ has a significant contribution from the relative stable $RC(O)OONO_2$ arising from the ring-opened acyl $C_{10}H_{15}O_8$-RO_2 reported by Iyer et al. (2021), its decomposition is relatively small (~21%). It should be noted that the RO_2 measured here is only a part of total RO_2 and that a large amount of RO_2 has already reacted to form closed-shell products as well as $ROONO_2$ in the flow reactor. Taking Exp 14 as an example (30 ppb NO_2), the simulated concentrations of RO_2 and $ROONO_2$ are 1.3 ppb and 1.9 ppb, which approximately accounts for 27.1% and 39.6% of the total production of RO_2, respectively. Therefore, the decomposition of $ROONO_2$ could indeed result in an increase in the RO_2 signal. It should also be pointed out that because of the very short residence time in the CI inlet, such an increase in the RO_2 concentration would not significantly impact HOM formation.

To confirm the reliability of our results, we examined the changes in the signals of RO_2 and closed-shell products as a function of reacted α-pinene in the absence of NO_2 (Section S1 and Figure S7), and the results are consistent with previous studies (Zhao et al., 2018). In addition, we repeated Exps 15-21 on another nitrate-CIMS and a similar increase in alkyl RO_2 signals with the addition of NO_2 was observed on that instrument (Figure S8).

3.2 Formation mechanisms of acyl RO_2 during α-pinene ozonolysis

It has been recently suggested that there are three main pathways that directly lead to the formation of monoterpene-derived acyl RO_2 (Zhao et al., 2022): (i) the autoxidation of RO_2 containing aldehyde groups (Reaction R1), (ii) the cleavage of C-C bond of RO containing an α-ketone group (Reaction R2), and (iii) the intramolecular H-shift of RO containing an aldehyde group (Reaction R3). In addition, the secondary OH oxidation of aldehyde products can also produce acyl RO_2 radicals. However, in the present study, the secondary OH oxidation is expected to be insignificant due to an excess of α-pinene compared to O_3. Indeed, kinetic model simulations incorporating the secondary OH chemistry show that the contribution of secondary OH oxidation to acyl RO_2 formation is negligible even under high O_3 conditions (see details in Section S2 and Figure S9).

Here, we further investigated the formation mechanisms of acyl RO_2. Figure 4 shows the reaction schemes leading to the formation of example acyl RO_2 radicals. The detailed formation mechanisms of acyl RO_2 measured in this study are shown in Figure S10. The formation of acyl RO_2, especially those having the small molecular size (C_7-C_9), requires the production and subsequent decomposition (or ring-opening process) of RO radicals. Take $C_8H_{13}O_6$-RO_2 as an example (Figure 4), two steps of RO formation and decomposition following the primary $C_{10}H_{15}O_4$-RO_2 lead to the ring-opened $C_8H_{13}O_4$-RO_2 that can undergo rapid aldehydic H-shift to form the acyl RO_2. While for $C_8H_{13}O_9$-RO_2, it directly comes from the aldehydic H-shift of $C_8H_{13}O_7$-RO followed by the O_2 addition (Figure S10).

$$RO_2 \xrightarrow{autox} acyl\ \ RO_2 \quad \text{(R1)}$$

$$RO_2 \xrightarrow{+RO_2} RO \xrightarrow{C-C\ cleavage} acyl\ \ RO_2 \quad \text{(R2)}$$

$$RO_2 \xrightarrow{+RO_2} RO \xrightarrow{H\ shift} acyl\ \ RO_2 \quad \text{(R3)}$$

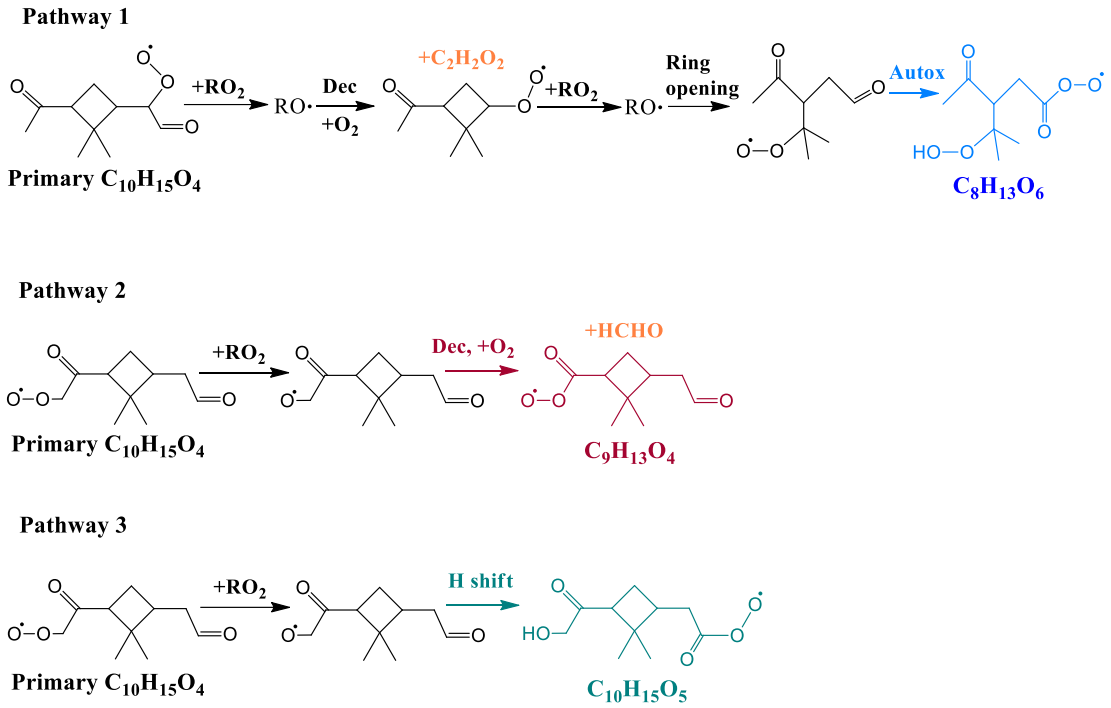

Figure 4 Three different formation pathways of acyl RO_2 during ozonolysis of α-pinene. The acyl RO_2, $C_9H_{13}O_4$ and $C_{10}H_{15}O_5$, formed via pathways 2 and 3, respectively, were not detected by nitrate-CIMS in this study due to their relatively low oxygenation level.

To verify the formation mechanisms of acyl RO_2, we added NO in some experiments (Exps 33-56) to see how acyl RO_2 respond to the increasing NO concentration. As shown in Figure 5, the changes of C_7 and C_8 acyl RO_2 show opposite trend with the increasing NO and NO_2 concentration, except for $C_8H_{13}O_8$-RO_2. NO can react with RO_2 to form RO radicals and promote the formation of RO_2 that requires the involvement of RO radicals in their formation. In addition to $C_8H_{13}O_6$-RO_2 discussed above, the formation of $C_7H_9O_7$-RO_2 and $C_8H_{13}O_9$-RO_2 needs 2 and 4 steps of the RO formation following $C_{10}H_{15}O_4$-RO_2 (Figure S10), respectively. Therefore, the increase of RO concentration due to the addition of NO would promote the production of these acyl RO_2. These results prove that the RO radicals indeed play an important role in the acyl RO_2 formation. While for $C_8H_{13}O_8$-RO_2, its signal decreases substantially with the addition of NO up to 3 ppb, similar to the trend observed with the addition of NO_2. After reaching the minimum at 7 ppb NO, the signal of $C_8H_{13}O_8$-RO_2 tends to increase with the further increase of NO concentration. Given that $C_8H_{13}O_8$-RO_2 is likely to directly come from the autoxidation of $C_8H_{13}O_6$ acyl RO_2 (see Figure S10), the rapid consumption of $C_8H_{13}O_6$-RO_2 by NO and NO_2 (formed by O_3 oxidation of NO) may outcompete its autoxidation process, thus leading to a decrease in $C_8H_{13}O_8$-RO_2 signal. Besides, it can be seen that the increasing extent in $C_8H_{13}O_6$-RO_2 is also relatively small before the NO concentration reaches 3 ppb (Figure 5c), indicating that the promotion effect of NO on $C_8H_{13}O_6$-

RO_2 formation is not that strong at this concentration.

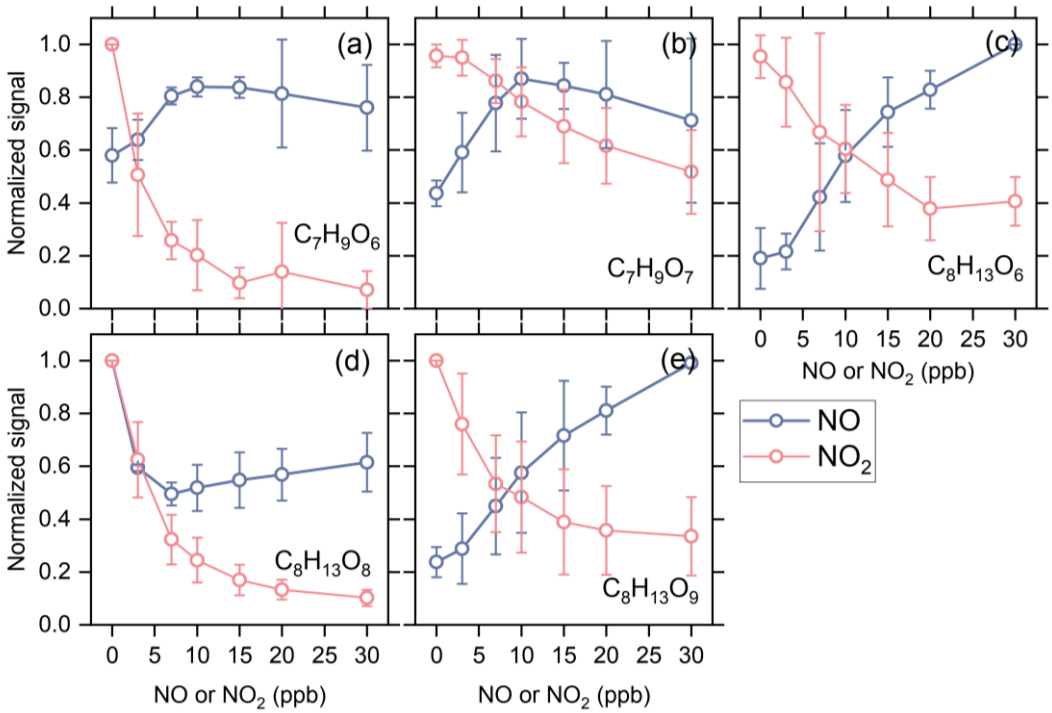

Figure 5 Averaged normalized signal of typical acyl RO_2 as a function of initial NO or NO_2 addition (Exps 1-28 and 33-56).

It is interesting to note that most of the measured highly oxygenated acyl RO_2 are formed by the autoxidation of aldehydic RO_2, and only the $C_8H_{13}O_9$-RO_2 is formed by the H-shift of the RO radical (Figure S10). The measured signal of acyl RO_2 from the autoxidation pathway accounts for 96% of all highly oxygenated acyl RO_2 signals. Considering that the acyl RO_2 with small molecular size are generally the ring-opened RO_2, the autoxidation rate constant of their precursor RO_2 is expected to be relatively high (e.g., 1 s^{-1}) (Iyer et al., 2021). Taking a RO_2 cross-reaction rate constant of 1×10^{-12} cm^3 $molecule^{-1}$ s^{-1} (Zhao et al., 2018) and a model-predicted total RO_2 concentration of 1.7 ppb (Exp 8), the simulated contributions of autoxidation and cross-reactions to the total RO_2 reaction are 96.0% and 4.0%, respectively. Considering a 10 times larger RO_2 cross-reaction rate constant (i.e., 1×10^{-11} cm^3 $molecule^{-1}$ s^{-1}), the simulated contributions of RO_2 autoxidation and cross-reactions would be 70.4% and 29.6%, respectively. These simulations suggest that the autoxidation of aldehydic RO_2 plays a dominant role in the formation of the highly oxygenated acyl RO_2. Although the acyl RO_2 with low oxygen content were not measured in this study, all acyl RO_2 containing oxygen atoms less than 6 seem to be derived from the cleavage of C-C bond or H-shift of RO containing an α-ketone or aldehyde in the currently known reaction mechanisms (Figures 4 and S11).

Recently, Shen et al. (2022) found that the hydrogen abstraction by OH radicals during α-pinene

oxidation plays an important role in HOM formation. In such mechanisms, the primary RO_2 reacts with NO and forms RO radicals, which could undergo rapid ring-breaking reactions to form a series of ring-opened $C_{10}H_{15}O_x$-RO_2, which contains aldehyde functionality and can easily autoxidize to C_{10} acyl RO_2. In the absence of NO, the cross-reactions of RO_2 can also produce RO radicals. However, only a few C_{10} acyl RO_2 were detected in this study and they contribute less than 1% of the total C_{10} RO_2 concentration. This phenomenon could be due to the fact that the primary RO_2 ($C_{10}H_{15}O_2$) formed by the hydrogen abstraction by OH radical are least-oxidized with only 2 oxygen atoms, which are expected to have a relatively low cross-reaction rate constant (Orlando and Tyndall, 2012; Berndt et al., 2018). As a result, the formation of ring-opened $C_{10}H_{15}O_x$-RO_2 via cross-reactions of the primary $C_{10}H_{15}O_2$-RO_2 may not be important. As shown in Figure 6, when the cross-reaction rate constants of $C_{10}H_{15}O_2$-RO_2 is considered to be 1×10^{-13} cm^3 $molecule^{-1}$ s^{-1}, the simulated contribution of the H-abstraction pathway to the HOM formation is less than 3% under both low (2.4 ppb) and high (9.6 ppb) reacted α-pinene conditions. It should be note that the cross-reaction rate constants of the less-oxygenated RO_2 could be even lower (Orlando and Tyndall, 2012), therefore the contribution of this pathway to HOM formation could be ignored when NO is absent.

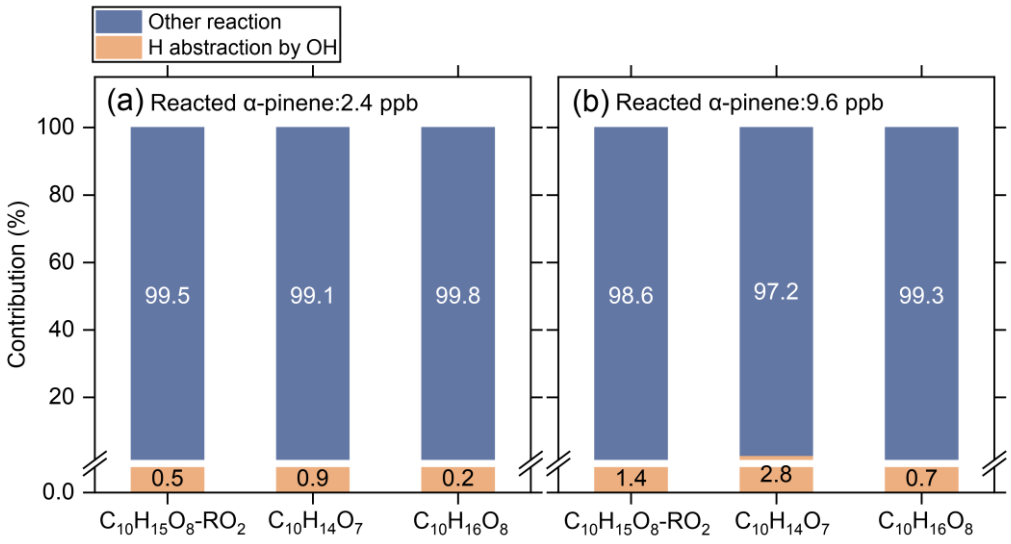

Figure 6 Contributions of the H-abstraction pathways by OH radicals (yellow) and OH addition and ozonolysis pathways (blue) to the formation of typical HOMs under low (a) and high (b) reacted α-pinene conditions simulated by the kinetic model. The cross-reaction rate constant was set to 1×10^{-13} cm^3 $molecule^{-1}$ s^{-1} for the primary $C_{10}H_{15}O_2$-RO_2 and 1×10^{-12} cm^3 $molecule^{-1}$ s^{-1} for the more oxygenated RO_2.

In the presence of cyclohexane as an OH scavenger (Figure S12, Exp 32), the measured signals of $C_{10}H_{17}O_x$-RO_2 formed via OH addition channel and the corresponding $C_{10}H_{18}O_x$-HOMs decrease by more than 70%, while the $C_{10}H_{15}O_x$-RO_2 and its related closed-shell products decrease by less

than 15%, in good agreement with the measurements in previous studies (Zhao et al., 2018). As the $C_{10}H_{16}O_8$-HOM could come from both $C_{10}H_{15}O_x$-RO_2 and $C_{10}H_{17}O_x$-RO_2, its reduction is at a medium level. The significantly smaller decrease in the signals of $C_{10}H_{15}O_x$-RO_2 and its corresponding closed-shell products as compared to those of $C_{10}H_{17}O_x$-RO_2 and the related closed-shell products further illustrates that the H-abstraction by OH has a minor contribution to HOM formation in the absence of NO.

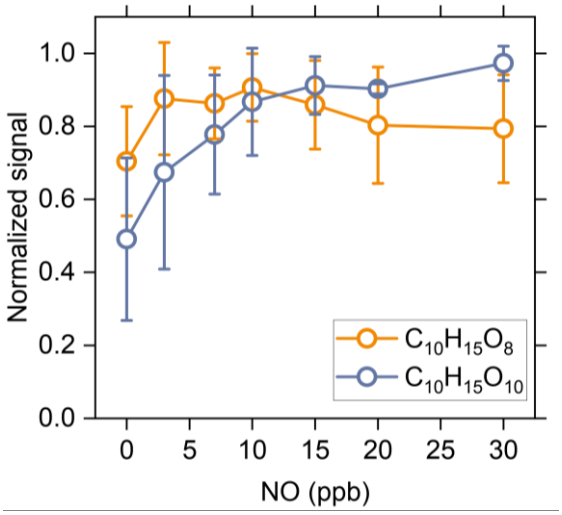

Figure 7 Averaged normalized signal of the measured $C_{10}H_{15}O_8$- and $C_{10}H_{15}O_{10}$-RO_2 as a function of the added NO concentration (Exps 33-56).

Figure 7 shows the changes in measured signal of $C_{10}H_{15}O_8$-RO_2 and $C_{10}H_{15}O_{10}$-RO_2 as a function of initial NO concentration (Exps 33-56). It should be noted that due to the existence of O_3 in our experiments, these two RO_2 could come from both O_3 and OH reactions with α-pinene and NO could be rapidly oxidized to NO_2 by O_3. The normalized signals of $C_{10}H_{15}O_8$-RO_2 and $C_{10}H_{15}O_{10}$-RO_2 increase firstly under low NO conditions, which is similar to the change of acyl RO_2 as shown in Figure 5. This increase could be due to two reasons: (1) the promoted formation of $C_{10}H_{15}O_8$ and $C_{10}H_{15}O_{10}$ acyl RO_2 from the H-abstraction channel by NO addition and (2) the equilibrium decomposition of $ROONO_2$ formed by the two alkyl RO_2 from ozonolysis of α-pinene in the CI inlet (see Section 3.1). As mentioned above, the ring-opened $C_{10}H_{15}O_x$-RO_2 formed from the H-abstraction channel contain aldehyde functionality and can autoxidize rapidly. The F0AM model simulations show that the $C_{10}H_{15}O_8$ and $C_{10}H_{15}O_{10}$ acyl RO_2 formed from the H-abstraction channel contribute to 68% and 56% of the total $C_{10}H_{15}O_8$-RO_2 and $C_{10}H_{15}O_{10}$-RO_2 with the addition of 10 ppb NO, respectively. Therefore, the initial increases of these two RO_2 with increasing NO concentration are likely mainly due to the enhanced formation of $C_{10}H_{15}O_8$ and $C_{10}H_{15}O_{10}$ acyl RO_2. When the NO concentration increases to a high level, there are more NO and NO_2 in the system, which promotes the consumption of acyl RO_2. As a result, $C_{10}H_{15}O_8$-RO_2 exhibits a decreasing trend

and the increasing extend of $C_{10}H_{15}O_{10}$-RO_2 becomes much smaller.

3.3 Contributions of acyl RO_2 to the formation of gas-phase HOMs

With the addition of NO_2, the distribution of gas-phase products in the α-pinene ozonolysis changes significantly (see Figure 1), and the consumption of acyl RO_2 by NO_2 plays an important role. NO_2 influences the formation of HOM monomers mainly in three ways. Firstly, NO_2 could react rapidly with acyl RO_2 and form $RC(O)OONO_2$, thus inhibiting the formation of HOMs with the involvement of acyl RO_2. Secondly, as mentioned above, although $ROONO_2$ is thermally unstable, their formation/decomposition equilibrium still consumes a small amount of alkyl RO_2, resulting in a decrease in HOM formation. Thirdly, NO_2 can consume a part of HO_2 radicals (Figure S13), thus inhibiting the $RO_2 + HO_2$ reaction pathway.

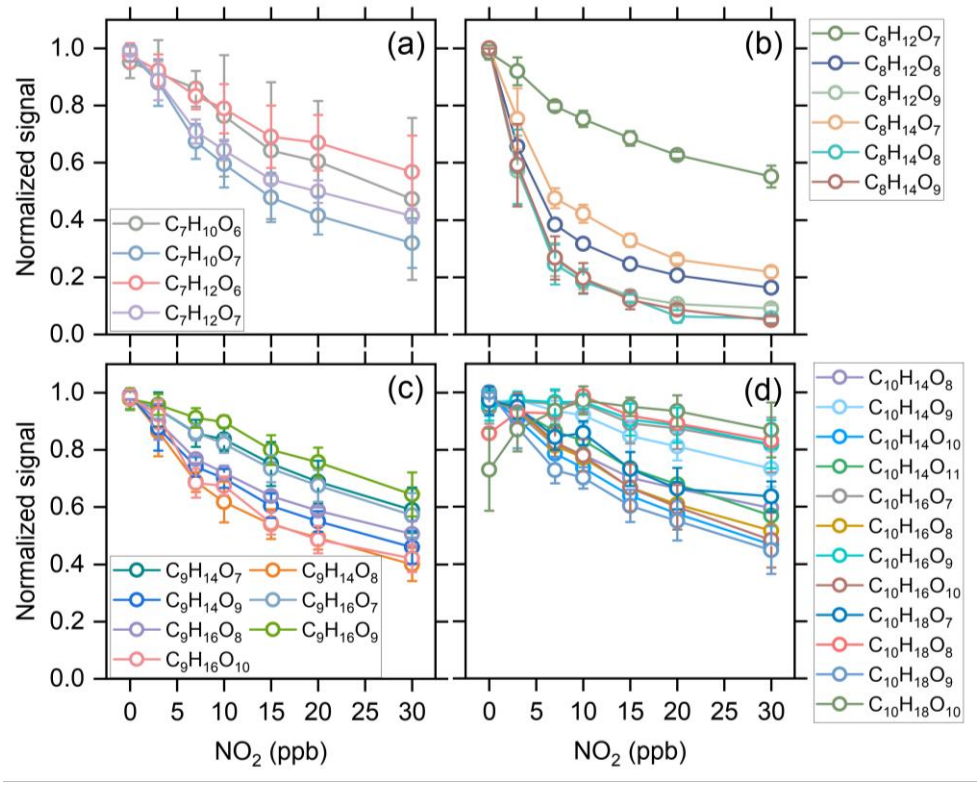

Figure 8 Averaged normalized signal of the measured C_7-C_{10} HOMs as a function of the added NO_2 concentration (Exps 1-28).

Figure 8 shows the normalized signal of C_7-C_{10} HOM monomers as a function of initial NO_2 concentration. The C_7, C_8, and some of C_9 HOMs decrease significantly with increasing NO_2 concentration due to the relatively large contribution of acyl RO_2 to the total C_7-C_9 RO_2. The C_7 HOMs decrease by more than 50% when the NO_2 concentration reaches 30 ppb, while C_8 HOMs decrease by more than 70% and some of them even decrease by 90%. The C_9 HOMs decrease by 30%-60% and the species with relatively large decrease are mostly acyl RO_2-related HOMs. For

C_{10} HOMs, although there is also an obvious decrease in their formation with the addition of NO_2, most of them have a smaller decreasing extent compared to the C_7-C_9 HOMs due to the low contribution of acyl RO_2 to the C_{10} RO_2. It is worth noting that a few C_{10} HOMs increase initially with the addition of NO_2 up to 10 ppb, suggesting that there might be some processes that promote the formation of their precursor RO_2 radicals and thus offset the inhibiting effect of NO_2.

As mentioned above, the addition of NO_2 has the most significant influence on the formation of small HOM monomers. Combined with the large contribution (67-94%) of acyl RO_2 to the total C_7 and C_8 RO_2 (Figure 3), it can be considered that the reduction in the formation of C_7 and C_8 HOM monomers with NO_2 addition is overwhelmingly due to the consumption of acyl RO_2 by NO_2. As a result, acyl RO_2 was found to have a contribution of 50-90% to C_7 and C_8 HOM monomer formation during α-pinene ozonolysis. Since acyl RO_2 also have a considerable contribution (32%) to the total C_9 RO_2, an upper limit (30%-60%) of its contribution to C_9 HOMs could be derived with the assumption that the decrease of C_9 HOMs with the addition of NO_2 is also mainly due to the consumption of C_9-acyl RO_2 by NO_2. By contrast, acyl RO_2 account for a very small fraction (0.4%) of the total C_{10} RO_2, and their contribution to C_{10} HOMs cannot be quantified based solely on the experimental measurements given that the equilibrium reaction between alkyl RO_2 and NO_2 can also affect the formation of HOMs. Therefore, we used the F0AM model to simulate the contribution of acyl RO_2 to C_{10} HOM formation according to the acyl RO_2 measured in this study and displayed the results in Figure 9. It should be noted that the HOMs from the acyl RO_2 and its subsequent RO_2 (formed from acyl RO_2 reactions) are all considered as acyl RO_2-related HOMs in the model.

As mentioned above, the formation of ring-opened $C_{10}H_{15}O_4$-RO_2 reported by Iyer et al. (2021) is included in the model, and its autoxidation produces a ring-opened acyl $C_{10}H_{15}O_8$-RO_2. When we consider the upper limit of the yield of ring-opened $C_{10}H_{15}O_4$-RO_2 (89%) in the model and assume that the other primary RO_2 with the cyclobutyl ring autoxidize at a very slow rate (0.01 s^{-1}), the simulated acyl $C_{10}H_{15}O_8$-RO_2 would contribute to ~80% of the total C_{10} RO_2. However, we could not see a large decrease in the measured signal of $C_{10}H_{15}O_8$-RO_2 and its related HOM monomers with the addition of NO_2. Similarly, a recent study by Zhao et al. (2022) found that the $C_{10}H_{15}O_8$-related monomers and dimers in α-pinene SOA did not significantly decrease with NO_2 addition. There might be three reasons for the discrepancy between the simulations and measurements. Firstly, the yield of the ring-opened $C_{10}H_{15}O_4$-RO_2 might be significantly smaller than 89% (Zhao et al., 2021; Meder et al., 2023). Secondly, the autoxidation rate of other primary $C_{10}H_{15}O_4$-RO_2 with the cyclobutyl ring could be significantly larger than 0.01 s^{-1}. Thirdly, the ring-opened $C_{10}H_{15}O_8$-RO_2, a highly functionalized acyl RO_2 radical with an –OOH group, may be able to undergo very fast

intramolecular H-scrambling reactions to form a peroxy acid as suggested by Knap and Jørgensen, (2017), which would compete with the NO_2 reaction and result in a lower reduction in its signal upon NO_2 addition (see details in Section S3).

To examine the contributions of acyl RO_2 to C_{10} HOM production, we updated the branching ratios and autoxidation rates of the primary RO_2 during α-pinene ozonolysis in the model according to the recent studies (Kurten et al., 2015; Claflin et al., 2018; Zhao et al., 2021; Berndt, 2022) (Table S3), and used a lower limit (30%) of the ring-opened $C_{10}H_{15}O_4$-RO_2 yield reported by Iyer et al. (2021). The simulated acyl RO_2-related HOMs contribute to 14% of the total C_{10} HOMs, which is slightly smaller than the measured decrease in C_{10} HOMs with the addition of NO_2. This discrepancy could be due to two reasons. Firstly, the decrease in HOMs can partly result from the consumption of alkyl RO_2 and HO_2 radicals by the addition of NO_2. Secondly, as mentioned above, there might be other C_{10} acyl RO_2 that were not observed in this study due to the decomposition of the $ROONO_2$ from the alkyl RO_2 with the same formulas. The contributions of acyl RO_2 to the formation of C_7-C_9 HOMs were also simulated (Figure 9). For C_7 and C_8 HOMs, the model predicts a contribution of 52%-98% from acyl RO_2, which is consistent with the measurements (50%-90%). However, the simulated contribution of acyl RO_2 to C_9 HOMs is over 99%, which is not consistent with the measurements (Figure 8c). Recent studies indicated that the CI radicals from α-pinene ozonolysis could not form the alkyl $C_9H_{15}O_3$-RO_2 (C96O2 in default MCM v3.3.1) (Kurten et al., 2015; Zhao et al., 2021; Berndt, 2022). As a result, this primary C_9 alkyl RO_2 was not considered in the model, and most of C_9 RO_2 considered are acyl RO_2 or from acyl RO_2 reactions. In view of the significantly lower measured (less than 30-60%) than simulated (over 99%) contribution of acyl RO_2 to C_9 HOMs, we speculate that a small part of CI radicals might be able to form the $C_9H_{15}O_3$-RO_2, which could further react to form highly oxygenated alkyl C_9 RO_2.

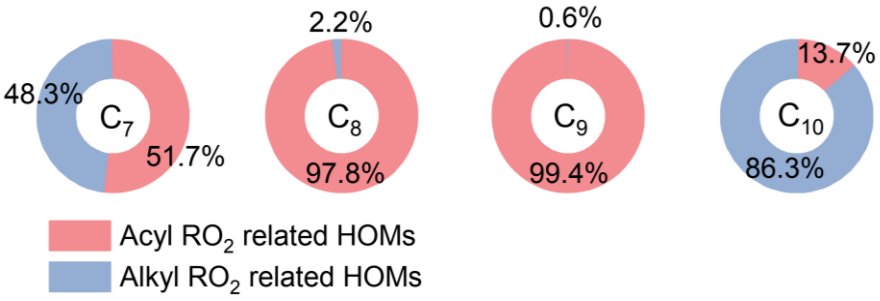

Figure 9 Simulated average contribution of acyl and alkyl RO_2 to C_7-C_{10} HOM formation from ozonolysis of α-pinene under typical experimental conditions (Exps 1, 8, 15, and 22).

A sensitivity analysis of the alkyl $C_9H_{15}O_3$-RO_2 yield was conducted to see its influence on the contribution of acyl RO_2 to the total C_9 HOMs. The model simulations show that when the yield of

this C_9 RO_2 from one of the CIs ranges between 0.5% to 2%, the contribution of acyl RO_2 to the total C_9 HOMs ranges from 27.5% to 59.8% (Figure S15), which is almost consistent with the measurements. This result indicates that a small part of CIs could generate the C_9 alkyl RO_2. We note that the small production of $C_9H_{15}O_3$-RO_2 from CIs has no significant influence on the yield of $C_{10}H_{15}O_4$-RO_2 and the subsequent acyl RO_2. As shown in Figure S16, as the $C_9H_{15}O_3$-RO_2 yield increases from 0% to 3%, the simulated concentrations of $C_{10}H_{15}O_4$-RO_2 exhibit negligible to small (5%) changes. As the $C_9H_{15}O_3$-RO_2 is considered to only produce highly oxygenated alkyl RO_2 in the model, it results in a decrease in the contribution of acyl RO_2 to the total C_9 HOMs. However, the contributions of acyl RO_2 to total C_7, C_8, and C_{10} HOMs are almost unchanged.

The cross-reaction rate constant of acyl RO_2 is generally larger than that of alkyl RO_2 (Atkinson et al., 2007; Orlando and Tyndall, 2012), and the fast cross-reaction may lead to an important contribution to the HOM dimer production. The responses of dimer formation to increasing concentration of initial NO_2 during α-pinene ozonolysis are given in Figure 10. The C_{14}-C_{18} dimers decrease by up to 50%-95% with the increase of NO_2 concentration up to 30 ppb (Figures 10a-e). The rapid cross-reaction rate of acyl RO_2, as well as their dominant contribution to the small RO_2 species makes acyl RO_2 an important contributor to the formation of these dimers. The consumption of acyl RO_2 by NO_2 greatly inhibits the bimolecular reactions involving acyl RO_2, resulting in a rapid decrease in the signal of the corresponding dimers. Considering the predominance of acyl RO_2 in small RO_2 and their high reaction rate with NO_2 compared to the alkyl RO_2, it can be concluded that the cross-reactions involving acyl RO_2 contribute to roughly 50%-95% of the C_{14}-C_{18} dimer formation.

For C_{19} dimers, due to the relatively smaller contribution of acyl RO_2 to C_9 and C_{10} RO_2, their signal decreases only by 10%-40%, and this reduction have contributions from both acyl and alkyl RO_2. For C_{20} dimers, their signal changes with the addition of NO_2 can be discussed according to the number of hydrogen atoms in the molecules. Firstly, the signal of $C_{20}H_{30}O_7$ and $C_{20}H_{30}O_9$ decreases by 40-60% with the addition of 30 ppb NO_2, indicating a significant contribution of acyl RO_2 such as $C_{10}H_{15}O_5$-RO_2 (acyl RO_2 in default MCM v3.3.1) and $C_{10}H_{15}O_7$-RO_2 in their formation, while other $C_{20}H_{30}O_x$ dimers decrease by ~30%. The $C_{20}H_{32}O_x$ dimer series also exhibits a small reduction (less than 20%) with the addition of NO_2. However, the $C_{20}H_{34}O_x$ series shows an unexpected increase with the addition of NO_2 up to 10 ppb and almost remains unchanged with the further increase of NO_2 concentration. Given that the cross-reaction rate constant of acyl RO_2 can be orders of magnitude higher than that of counterpart alkyl RO_2 (Atkinson et al., 2007; Orlando and Tyndall, 2012), the rapid consumption of acyl RO_2 by NO_2 would preserve the alkyl RO_2 that tend to react

with acyl RO_2 at a fast rate in the absence of NO_2, which to some extent would elevate the concentration of alkyl RO_2 in the system and thus promote the less competitive alkyl RO_2 + alkyl RO_2 reactions to form $C_{20}H_{34}O_x$ dimers. The slight increase of some $C_{10}H_{18}O_x$-HOMs with the addition of NO_2 up to 10 ppb could also be due to this reason.

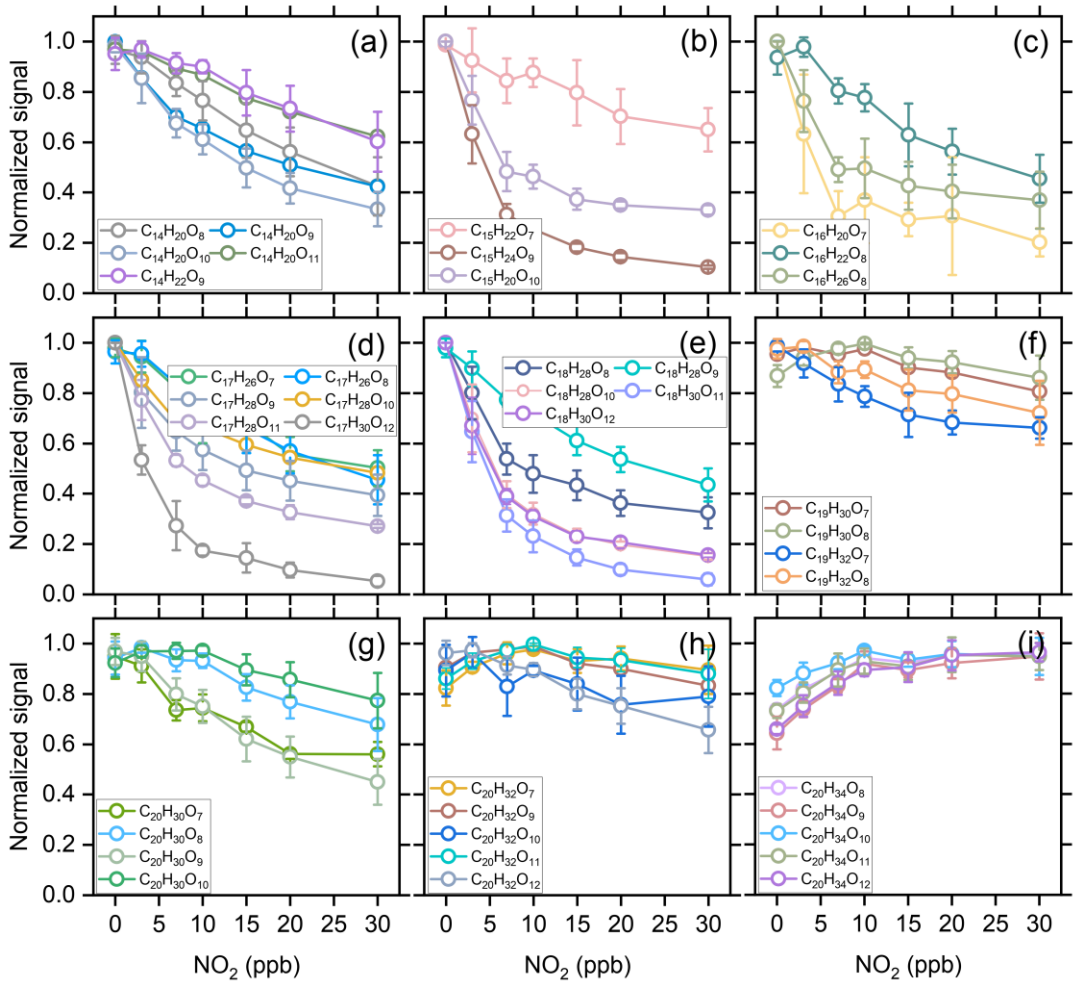

Figure 10 Averaged normalized signal of the measured C_{14}-C_{20} dimers as a function of the added NO_2 concentration (Exps 1-28).

According to the noticeable increasing trend in $C_{20}H_{34}O_x$ as compared to other C_{20} dimers, we speculate that acyl RO_2 react faster with $C_{10}H_{17}O_x$ alkyl RO_2 than with $C_{10}H_{15}O_x$ alkyl RO_2. Therefore, when the acyl RO_2 is depleted, the preservation of $C_{10}H_{17}O_x$-RO_2 is more significant and the promotion of their cross-reactions to form $C_{20}H_{34}O_x$ is more evident. It is also possible that the reaction of NO_2 with $C_{10}H_{17}O_x$ alkyl RO_2 is less efficient compared to the reaction with $C_{10}H_{15}O_x$ alkyl RO_2, so more $C_{10}H_{17}O_x$ than $C_{10}H_{15}O_x$ are available for dimer formation in the presence of NO_2.

To further prove the above two speculations, we performed sensitivity analyses for the reaction rates

of $C_{10}H_{17}O_x$-RO_2 using the F0AM model. Figures 11a show the changes in $C_{20}H_{34}O_x$ dimers with NO_2 addition at different $C_{10}H_{17}O_x$-RO_2 + NO_2 reaction rates under the conditions of Exps 8-14. As the reaction rate varies from 1×10^{-13} to 1×10^{-12} cm^3 $molecule^{-1}$ s^{-1}, the increasing trend of $C_{20}H_{34}O_x$ dimers versus the added NO_2 concentration is weakened and the simulation is more deviated from the measurements. When the reaction rate increases to 7.5×10^{-12} cm^3 $molecule^{-1}$ s^{-1}, the $C_{20}H_{34}O_x$ dimers decrease significantly with increasing NO_2, which is in striking contrast to the measurements. Figure 11b presents the sensitivity analysis results for the cross-reaction rate constants of acyl RO_2 + $C_{10}H_{17}O_x$-RO_2. As this rate constant varies from 1×10^{-12} to 1×10^{-10} cm^3 $molecule^{-1}$ s^{-1}, the increasing trend of $C_{20}H_{34}O_x$ versus the NO_2 concentration is more pronounced and more consistent with the measurements. These sensitivity analyses support our speculation that the $C_{10}H_{17}O_x$ alkyl RO_2 may be different from other alkyl RO_2 radicals in terms of the reaction efficiency with NO_2 and acyl RO_2 species, which leads to different responses of $C_{20}H_{34}O_x$ dimers to NO_2 addition compared to other C_{20} dimers. These results also suggest that the presence of acyl RO_2 could affect the fate and contribution of alkyl RO_2 to HOM formation in atmospheric oxidation systems given the different reactivity of acyl RO_2 from alkyl RO_2.

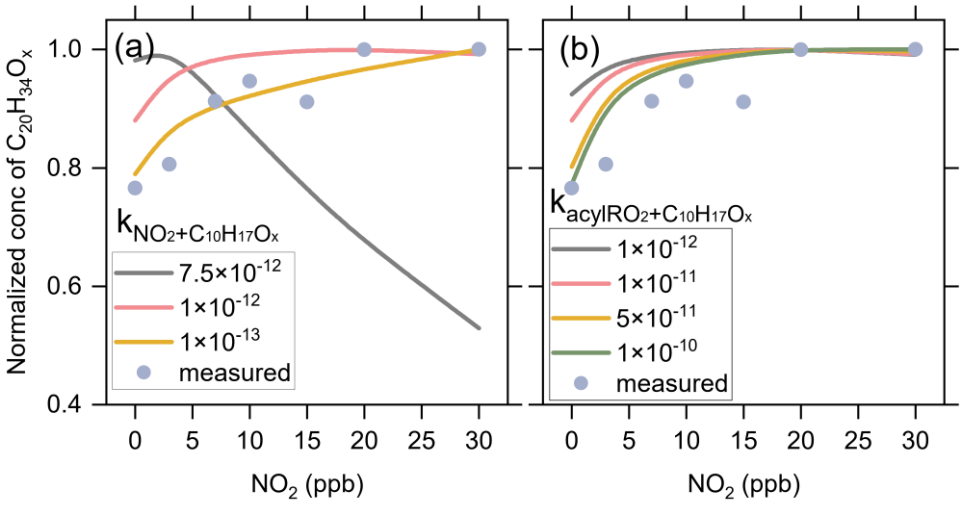

Figure 11 Sensitivity of $C_{20}H_{34}O_x$ dimer production to (a) the reaction rates of NO_2 with $C_{10}H_{17}O_x$-RO_2 and (b) the cross-reaction rate of acyl RO_2 with $C_{10}H_{17}O_x$-RO_2 considering a $C_{10}H_{17}O_x$-RO_2 + NO_2 reaction rate of 1×10^{-12} cm^3 $molecule^{-1}$ s^{-1}.

4. Conclusions

In this study, the molecular identities, formation mechanisms, and contributions of acyl RO_2 to the formation of HOMs during ozonolysis of α-pinene are investigated using a combination of flow reactor experiments and detailed kinetic model simulations. Based on the marked decrease in RO_2 signal as a function of initial NO_2 concentration, a total of 10 acyl RO_2 are identified during α-

pinene ozonolysis. The acyl RO_2 contributes to 67%, 94% and 32% of C_7, C_8 and C_9 highly oxygenated RO_2 but only 0.4% of C_{10} highly oxygenated RO_2, respectively. Three main pathways are identified for the formation of monoterpene-derived acyl RO_2: (i) the autoxidation of RO_2 containing aldehyde groups, (ii) the cleavage of C-C bond of RO containing an α-ketone group, and (iii) the intramolecular H-shift of RO containing an aldehyde group. The autoxidation of aldehydic RO_2 formed involving multiple RO decomposition or ring-opening steps plays a dominant role in the formation of the highly oxygenated acyl RO_2 radicals (oxygen atom number ≥ 6), while the less-oxygenated acyl RO_2 (oxygen atom number < 6) are mainly derived from the other two pathways.

The acyl RO_2-involved reactions explain 50-90% of C_7 and C_8 HOM monomers and 14% of C_{10} HOMs, respectively. For C_9 HOMs, this contribution can be up to 30%-60%. For the HOM dimers, acyl RO_2-involved reactions contribute 50%-95% to the formation of C_{14}-C_{18} dimers. Owing to the higher cross-reaction rate constant of acyl RO_2 compared to alkyl RO_2, the acyl RO_2 + alkyl RO_2 reaction would outcompete the alkyl RO_2 + alkyl RO_2 reaction. Therefore, the rapid consumption of acyl RO_2 by NO_2 in the experiments (as well as in polluted atmospheres) would make the alkyl RO_2 that are supposed to react with acyl RO_2 retained, which to some extent elevates the concentration of alkyl RO_2 in the system and thus promotes the reaction of alkyl RO_2 + alkyl RO_2 to form dimers such as $C_{20}H_{34}O_x$. The contribution of H-abstraction of α-pinene by OH radical to the formation of acyl RO_2 and HOMs is found to be negligible in the absence of NO. This is because the primary $C_{10}H_{15}O_2$-RO_2 radicals formed in such pathways are least-oxidized and thus have relatively low cross-reaction efficiency to produce RO radicals, which are the key intermediates for the formation of acyl RO_2 and HOMs in that channel. However, in the presence of NO, the formation of highly oxygenated acyl RO_2 via the H-abstraction pathway is demonstrated, consistent with previous studies (Shen et al., 2022).

In this study, acyl RO_2 species are identified according to a dramatic decrease in their signal with the addition of NO_2. It should be noted that the presence of NO_2 could also inhibit the formation of alkyl RO_2 species involving acyl RO_2 reactions. If there are any contributions of alkyl RO_2 to acyl RO_2 identified in this study, the influence of such alkyl RO_2 species on HOM formation would reflect an indirect effect of acyl RO_2. However, given that the formation of most of the acyl RO_2 identified in this study can be reasonably explained by the proposed mechanisms and verified by their responses to the addition of NO, the acyl RO_2 identified here are expected to have no significant contributions from alkyl RO_2. Currently, the reaction kinetics of monoterpene-derived acyl RO_2 are still poorly understood. Considering the important contribution of acyl RO_2 to HOM formation, further kinetic studies are needed to get more specific rate constants for their autoxidation and cross-

reactions, thereby deepening our understanding of the role of acyl RO_2 in HOM and SOA formation under atmospheric conditions.

Data availability. The data presented in this work are available upon request from the corresponding author.

Author contributions. YZ and HZ designed the study, HZ, DH and JZ performed the experiments. YZ and HZ analyzed the data, conducted model simulations, and wrote the paper. All other authors contributed to discussion and writing.

Competing interests. The authors declare no conflict of interest.

Acknowledgments. Yue Zhao acknowledges the Program for Professor of Special Appointment (Eastern Scholar) at Shanghai Institutions of Higher Learning.

Financial support. This work was supported by the National Natural Science Foundation of China (grants 22022607, 21806104, and 42005090) and the Program for Professor of Special Appointment (Eastern Scholar) at Shanghai Institutions of Higher Learning.

References

Atkinson, R., Hasegawa, D., and Aschmann, S. M.: Rate constants for the gas-phase reactions of O_3 with a series of monoterpenes and related compounds at 296 ± 2 K, Int. J. Chem. Kinet., 1221, https://doi.org/10.1002/kin.550220807, 1990.

Atkinson, R., Baulch, D., Cox, R., Crowley, J., Hampson, R., Hynes, R., Jenkin, M., Rossi, M., and Troe, J.: Evaluated kinetic and photochemical data for atmospheric chemistry: Volume III–gas phase reactions of inorganic halogens, Atmos. Chem. Phys., 7, 981-1191, https://doi.org/10.5194/acp-7-981-2007, 2007.

Bell, D. M., Wu, C., Bertrand, A., Graham, E., Schoonbaert, J., Giannoukos, S., Baltensperger, U., Prevot, A., Riipinen, I., and Haddad, I. E.: Particle-phase processing of α-pinene NO_3 secondary organic aerosol in the dark, Atmos. Chem. Phys., 13167–13182, https://doi.org/10.5194/acp-22-13167-2022, 2021.

Berndt, T.: Peroxy radical processes and product formation in the OH radical-initiated oxidation of alpha-pinene for near-atmospheric conditions, J. Phys. Chem. A, 125, 9151-9160, https://doi.org/10.1021/acs.jpca.1c05576, 2021.

Berndt, T.: Peroxy radical and product formation in the gas-phase ozonolysis of alpha-pinene under near-atmospheric conditions: occurrence of an additional series of peroxy radicals O,O-C10H15O(O2)yO2 with y = 1-3, J. Phys. Chem. A, 126, 6526-6537, https://doi.org/10.1021/acs.jpca.2c05094, 2022.

Berndt, T., Mentler, B., Scholz, W., Fischer, L., Herrmann, H., Kulmala, M., and Hansel, A.: Accretion product formation from ozonolysis and OH radical reaction of alpha-pinene: mechanistic insight and the influence of isoprene and ethylene, Environ. Sci. Technol., 52, 11069-11077,

https://doi.org/10.1021/acs.est.8b02210, 2018.

Berndt, T., Richters, S., Jokinen, T., Hyttinen, N., Kurtén, T., Otkjær, R. V., Kjaergaard, H. G., Stratmann, F., Herrmann, H., and Sipilä, M.: Hydroxyl radical-induced formation of highly oxidized organic compounds, Nat. Commun., 7, 1-8, https://doi.org/10.1038/ncomms13677, 2016.

Bianchi, F., Kurtén, T., Riva, M., Mohr, C., Rissanen, M. P., Roldin, P., Berndt, T., Crounse, J. D., Wennberg, P. O., and Mentel, T. F.: Highly oxygenated organic molecules (HOM) from gas-phase autoxidation involving peroxy radicals: A key contributor to atmospheric aerosol, Chem. Rev., 119, 3472-3509, 2019.

Calvert, J. G., Derwent, R. G., Orlando, J. J., Wallington, T. J., and Tyndall, G. S.: Mechanisms of atmospheric oxidation of the alkanes, 2008.

Claflin, M. S., Krechmer, J. E., Hu, W., Jimenez, J. L., and Ziemann, P. J.: Functional group composition of secondary organic aerosol formed from ozonolysis of α-pinene under high VOC and autoxidation conditions, ACS Earth Space Chem., 2, 1196-1210, https://doi.org/10.1021/acsearthspacechem.8b00117, 2018.

Ehn, M., Thornton, J. A., Kleist, E., Sipilä, M., Junninen, H., Pullinen, I., Springer, M., Rubach, F., Tillmann, R., and Lee, B.: A large source of low-volatility secondary organic aerosol, Nature, 506, 476-479, https://doi.org/10.1038/nature13032, 2014.

Fry, J., Kiendler-Scharr, A., Rollins, A., Wooldridge, P., Brown, S., Fuchs, H., Dubé, W., Mensah, A., Dal Maso, M., and Tillmann, R.: Organic nitrate and secondary organic aerosol yield from NO_3 oxidation of β-pinene evaluated using a gas-phase kinetics/aerosol partitioning model, Atmos. Chem. Phys., 9, 1431-1449, https://doi.org/10.5194/acp-9-1431-2009, 2009.

Fry, J. L., Draper, D. C., Barsanti, K. C., Smith, J. N., Ortega, J., Winkler, P. M., Lawler, M. J., Brown, S. S., Edwards, P. M., and Cohen, R. C.: Secondary organic aerosol formation and organic nitrate yield from NO_3 oxidation of biogenic hydrocarbons, Environ. Sci. Technol., 48, 11944-11953, https://doi.org/10.1021/es502204x, 2014.

Guenther, A., Jiang, X., Heald, C. L., Sakulyanontvittaya, T., Duhl, T. a., Emmons, L., and Wang, X.: The model of emissions of gases and aerosols from nature version 2.1 (MEGAN2. 1): an extended and updated framework for modeling biogenic emissions, Geosci. Model Dev., 5, 1471-1492, https://doi.org/10.5194/gmd-5-1471-2012, 2012.

Iyer, S., Rissanen, M. P., Valiev, R., Barua, S., Krechmer, J. E., Thornton, J., Ehn, M., and Kurten, T.: Molecular mechanism for rapid autoxidation in alpha-pinene ozonolysis, Nat. Commun., 12, 878, https://doi.org/10.1038/s41467-021-21172-w, 2021.

Jenkin, M., Young, J., and Rickard, A.: The MCM v3.3.1 degradation scheme for isoprene, Atmos. Chem. Phys., 15, 11433-11459, https://doi.org/10.5194/acp-15-11433-2015, 2015.

Jokinen, T., Sipilä, M., Richters, S., Kerminen, V. M., Paasonen, P., Stratmann, F., Worsnop, D., Kulmala, M., Ehn, M., and Herrmann, H.: Rapid autoxidation forms highly oxidized RO_2 radicals in the atmosphere, Angew. Chem. Int. Ed., 53, 14596-14600, https://doi.org/10.1002/anie.201408566, 2014.

Junninen, H., Ehn, M., Petäjä, T., Luosujärvi, L., Kotiaho, T., Kostiainen, R., Rohner, U., Gonin, M., Fuhrer, K., and Kulmala, M.: A high-resolution mass spectrometer to measure atmospheric ion composition, Atmos. Meas. Tech., 3, 599-636, https://doi.org/10.5194/amt-3-1039-2010, 2010.

Kirchner, F., Thuener, L., Barnes, I., Becker, K., Donner, B., and Zabel, F.: Thermal lifetimes of peroxynitrates occurring in the atmospheric degradation of oxygenated fuel additives, Environ. Sci. Technol., 31, 1801-1804, https://doi.org/10.1021/es9609415, 1997.

Knap, H. C. and Jørgensen, S.: Rapid Hydrogen Shift Reactions in Acyl Peroxy Radicals, J. Phys. Chem. A, 121, 1470-1479, 10.1021/acs.jpca.6b12787, 2017.

Knopf, D. A., Pöschl, U., and Shiraiwa, M.: Radial diffusion and penetration of gas molecules and aerosol particles through laminar flow reactors, denuders, and sampling tubes, Anal. Chem., 87, 3746-3754, https://doi.org/10.1021/ac5042395, 2015.

Kristensen, K., Watne, Å. K., Hammes, J., Lutz, A., Petäjä, T., Hallquist, M., Bilde, M., and Glasius, M.: High-molecular weight dimer esters are major products in aerosols from α-pinene ozonolysis and the boreal forest, Environ. Sci. Technol. Lett., 3, 280-285, 2016.

Kurten, T., Rissanen, M. P., Mackeprang, K., Thornton, J. A., Hyttinen, N., Jorgensen, S., Ehn, M., and Kjaergaard, H. G.: Computational study of hydrogen shifts and ring-opening mechanisms in alpha-pinene ozonolysis products, J. Phys. Chem. A, 119, 11366-11375, https://doi.org/10.1021/acs.jpca.5b08948, 2015.

Li, X., Chee, S., Hao, J., Abbatt, J. P. D., Jiang, J., and Smith, J. N.: Relative humidity effect on the formation of highly oxidized molecules and new particles during monoterpene oxidation, Atmos. Chem. Phys., 19, 1555-1570, https://doi.org/10.5194/acp-19-1555-2019, 2019.

Lin, C., Huang, R.-J., Duan, J., Zhong, H., and Xu, W.: Primary and secondary organic nitrate in northwest China: a case study, Environ. Sci. Technol. Lett., 8, 947-953, https://doi.org/10.1021/acs.estlett.1c00692, 2021.

Meder, M., Peräkylä, O., Varelas, J. G., Luo, J., Cai, R., Zhang, Y., Kurtén, T., Riva, M., Rissanen, M., Geiger, F. M., Thomson, R. J., and Ehn, M.: Selective deuteration as a tool for resolving autoxidation mechanisms in α-pinene ozonolysis, Atmos. Chem. Phys., 23, 4373-4390, https://doi.org/10.5194/egusphere-2022-1131, 2023.

Mentel, T., Springer, M., Ehn, M., Kleist, E., Pullinen, I., Kurtén, T., Rissanen, M., Wahner, A., and Wildt, J.: Formation of highly oxidized multifunctional compounds: autoxidation of peroxy radicals formed in the ozonolysis of alkenes–deduced from structure–product relationships, Atmos. Chem. Phys., 15, 6745-6765, https://doi.org/10.5194/acp-15-6745-2015, 2015.

Molteni, U., Simon, M., Heinritzi, M., Hoyle, C. R., Bernhammer, A.-K., Bianchi, F., Breitenlechner, M., Brilke, S., Dias, A., Duplissy, J., Frege, C., Gordon, H., Heyn, C., Jokinen, T., Kürten, A., Lehtipalo, K., Makhmutov, V., Petäjä, T., Pieber, S. M., Praplan, A. P., Schobesberger, S., Steiner, G., Stozhkov, Y., Tomé, A., Tröstl, J., Wagner, A. C., Wagner, R., Williamson, C., Yan, C., Baltensperger, U., Curtius, J., Donahue, N. M., Hansel, A., Kirkby, J., Kulmala, M., Worsnop, D. R., and Dommen, J.: Formation of highly oxygenated organic molecules from α-pinene ozonolysis: chemical characteristics, mechanism, and kinetic model development, ACS Earth Space Chem., 3, 873-883, https://doi.org/10.1021/acsearthspacechem.9b00035, 2019.

Noziere, B., Kalberer, M., Claeys, M., Allan, J., D'Anna, B., Decesari, S., Finessi, E., Glasius, M., Grgic, I., and Hamilton, J. F.: The molecular identification of organic compounds in the atmosphere: state of the art and challenges, Chem. Rev., 115, 3919-3983, 2015.

Orlando, J. J. and Tyndall, G. S.: Laboratory studies of organic peroxy radical chemistry: an overview with emphasis on recent issues of atmospheric significance, Chem. Soc. Rev., 41, 6294-6317, https://doi.org/10.1039/C2CS35166H, 2012.

Otkjær, R. V., Jakobsen, H. H., Tram, C. M., and Kjaergaard, H. G.: Calculated hydrogen shift rate constants in substituted alkyl peroxy radicals, J. Phys. Chem. A, 122, 8665-8673, https://doi.org/10.1021/acs.jpca.8b06223, 2018.

Pye, H., Chan, A., Barkley, M., and Seinfeld, J.: Global modeling of organic aerosol: the importance of

reactive nitrogen (NO_x and NO_3), Atmos. Chem. Phys., 10, 11261-11276, https://doi.org/10.5194/acp-10-11261-2010, 2010.

Roger, Atkinson, Sara, M., Aschmann, James, N., Pitts, and Jr.: Rate constants for the gas-phase reactions of the OH radical with a series of monoterpenes at 294 ± 1 K, Int. J. Chem. Kinet., 2004.

Shen, H., Vereecken, L., Kang, S., Pullinen, I., Fuchs, H., Zhao, D., and Mentel, T. F.: Unexpected significance of a minor reaction pathway in daytime formation of biogenic highly oxygenated organic compounds, Sci. Adv., 8, eabp8702, https://doi.org/10.1126/sciadv.abp8702, 2022.

Sindelarova, K., Granier, C., Bouarar, I., Guenther, A., Tilmes, S., Stavrakou, T., Müller, J.-F., Kuhn, U., Stefani, P., and Knorr, W.: Global data set of biogenic VOC emissions calculated by the MEGAN model over the last 30 years, Atmos. Chem. Phys., 14, 9317-9341, https://doi.org/10.5194/acp-14-9317-2014, 2014.

Tyndall, G., Cox, R., Granier, C., Lesclaux, R., Moortgat, G., Pilling, M., Ravishankara, A., and Wallington, T.: Atmospheric chemistry of small organic peroxy radicals, J. Geophys. Res.-Atmos., 106, 12157-12182, 2001.

Villenave, E. and Lesclaux, R.: Kinetics of the cross reactions of CH_3O_2 and $C_2H_5O_2$ radicals with selected peroxy radicals, J. Phys. Chem. C, 100, 14372-14382, https://doi.org/10.1021/jp960765m, 1996.

Wang, Y., Zhao, Y., Li, Z., Li, C., Yan, N., and Xiao, H.: Importance of hydroxyl radical chemistry in isoprene suppression of particle formation from α-pinene ozonolysis, ACS Earth Space Chem., 5, 487-499, https://doi.org/10.1021/acsearthspacechem.0c00294, 2021.

Wolfe, G. M., Marvin, M. R., Roberts, S. J., Travis, K. R., and Liao, J.: The framework for 0-D atmospheric modeling (F0AM) v3. 1, Geosci. Model Dev., 9, 3309-3319, https://doi.org/10.5194/gmd-9-3309-2016, 2016.

Xu, L., Møller, K. H., Crounse, J. D., Otkjær, R. V., Kjaergaard, H. G., and Wennberg, P. O.: Unimolecular reactions of peroxy radicals formed in the oxidation of α-pinene and β-pinene by hydroxyl radicals, J. Phys. Chem. A, 123, 1661-1674, https://doi.org/10.1021/acs.jpca.8b11726, 2019.

Yao, M., Zhao, Y., Hu, M., Huang, D., and Yan, N.: Multiphase reactions between secondary organic aerosol and sulfur dioxide: kinetics and contributions to sulfate formation and aerosol aging, Environ. Sci. Technol. Lett., https://doi.org/10.1021/acs.estlett.9b00657, 2019.

Zhang, H., Yee, L. D., Lee, B. H., Curtis, M. P., Worton, D. R., Isaacman-VanWertz, G., Offenberg, J. H., Lewandowski, M., Kleindienst, T. E., and Beaver, M. R.: Monoterpenes are the largest source of summertime organic aerosol in the southeastern United States, Proc. Natl. Acad. Sci. U. S. A. , 115, 2038-2043, https://doi.org/10.1073/pnas.1717513115, 2018.

Zhao, Y., Thornton, J. A., and Pye, H. O. T.: Quantitative constraints on autoxidation and dimer formation from direct probing of monoterpene-derived peroxy radical chemistry, Proc. Natl. Acad. Sci. U. S. A. , 115, 12142-12147, https://doi.org/10.1073/pnas.1812147115, 2018.

Zhao, Y., Yao, M., Wang, Y. Q., Li, Z. Y., Wang, S. Y., Li, C. X., and Xiao, H. Y.: Acylperoxy Radicals as Key Intermediates in the Formation of Dimeric Compounds in alpha-Pinene Secondary Organic Aerosol, Environ. Sci. Technol., 56, 14249-14261, 10.1021/acs.est.2c02090, 2022.

Zhao, Z. X., Zhang, W., Alexander, T., Zhang, X., Martin, D. B. C., and Zhang, H. F.: Isolating a-Pinene Ozonolysis Pathways Reveals New Insights into Peroxy Radical Chemistry and Secondary Organic Aerosol Formation, Environ. Sci. Technol., 55, 6700-6709, 10.1021/acs.est.1c02107, 2021.